SUPPLEMENTARY INFORMATION

Structural diversity in proline-based lead bromide chiral perovskites

Valerii Y. Sirenko,[a] Olesia I. Kucheriv,[a] Igor O. Fritsky,[a] Elzbieta Gumienna-Kontecka,[b] Ioan-Andrei Dascălu,[c] Sergiu Shova,[c] and Il'ya A. Gural'skiy*[a]

a. Department of Chemistry, Taras Shevchenko National University of Kyiv, Volodymyrska St. 64, 01601 Kyiv, Ukraine. E-mail: illia.guralskyi@univ.kiev.ua

b. Faculty of Chemistry, University of Wrocław, F. Joliot-Curie 14, 50383 Wrocław, Poland

c. Department of Inorganic Polymers, "Petru Poni" Institute of Macromolecular Chemistry, 41A Aleea Gr. Ghica Voda, 700487 Iasi, Romania

Corresponding Author

*E-mail address: illia.guralskyi@univ.kiev.ua

Table S1. The Σ, Δd and σ^2 values for previously reported hybrid perovskites

	(API)$PbBr_4$ [1]	(*R*/*S*-2-MPD)$PbBr_3$ [2]	$(CH_3)_3SPbI_3$ [3]	$[C_2H_7N_2][PbI_3]$ [4]	$(tms)_4Pb_3Br_{10}$ [5]
Σ, °	45.07	105.29	54.32	70.64	$Pb(1)Br_6$ = 64.51; $Pb(2)Br_6$ = 87.66
Δd	$2.6\cdot10^{-3}$	$4.5\cdot10^{-3}$	$5.5\cdot10^{-5}$	$1.2\cdot10^{-7}$	$Pb(1)Br_6 = 1.4\cdot10^{-3}$; $Pb(2)Br_6 = 3.9\cdot10^{-5}$
σ^2, (°)^2	20.8	115.86	22.69	39.06	$Pb(1)Br_6$ = 45.37; $Pb(2)Br_6$ = 59.35

Table S2. Selected bond lengths (Å) for **Pro-$PbBr_3$** and **Pro-Pb_3Br_{10}**

Pro-$PbBr_3$			
Pb1−Br4	2.9349(19)	Pb2−Br6	2.9288(19)
Pb1−Br2	2.961(2)	Pb2−Br5	2.940(2)
Pb1−Br1	2.999(2)	Pb2−Br3	3.038(2)
Pb1−Br5	3.023(2)	Pb2−Br2^2	3.064(2)
Pb1−Br6^1	3.1375(19)	Pb2−Br1^2	3.141(2)
Pb1−Br3	3.146(2)	Pb2−Br4	3.151(2)
^{1} −1 + x, +y, +z; ^{2} 1 + x, +y, +z			
Pro-Pb_3Br_{10}			
Pb2−Br2	2.9311(16)	Pb1−Br2^2	3.0451(17)
Pb2−Br1	3.0957(14)	Pb1−Br2	3.0451(17)
Pb2−Br3	3.1178(17)	Pb1−Br1	3.0206(14)
Pb2−Br4	2.9713(18)	Pb1−Br1^2	3.0207(14)
Pb2−Br4^1	3.1268(19)	Pb1−Br3^2	3.0091(18)
Pb2−Br5	2.9671(15)	Pb1−Br3	3.0091(18)
^{1} 1.5 − x, −0.5 + y, 1 − z; ^{2} 1 − x, y, 1 − z; ^{3}1.5 − x, 0.5 + y, 1 − z.			

Table S3. Selected bond angles (°) for **Pro-$PbBr_3$** and **Pro-Pb_3Br_{10}**

Pro-$PbBr_3$			
Br4–Pb1–Br2	89.49(6)	Br6–Pb2–Br2^2	84.68(5)
Br4–Pb1–Br1	91.54(6)	Br5–Pb2–Br2^2	101.41(7)
Br2–Pb1–Br1	82.33(6)	Br3–Pb2–Br2^2	170.97(6)
Br4–Pb1–Br5	85.50(6)	Br6–Pb2–Br1^2	85.67(6)
Br2–Pb1–Br5	101.93(7)	Br5–Pb2–Br1^2	175.46(6)
Br1–Pb1–Br5	174.77(6)	Br3–Pb2–Br1^2	93.02(6)
Br4–Pb1–Br6^1	171.83(6)	Br2^2–Pb2–Br1^2	78.41(6)
Br2–Pb1–Br6^1	82.88(5)	Br6–Pb2–Br4	172.76(6)
Br1–Pb1–Br6^1	84.56(5)	Br5–Pb2–Br4	83.15(5)
Br5–Pb1–Br6^1	98.90(6)	Br3–Pb2–Br4	80.43(5)
Br4–Pb1–Br3	82.11(5)	Br2^2–Pb2–Br4	98.30(5)
Br2–Pb1–Br3	169.35(6)	Br1^2–Pb2–Br4	101.37(6)
Br1–Pb1–Br3	91.33(6)	Pb1–Br2–Pb2^1	80.86(5)
Br5–Pb1–Br3	84.00(6)	Pb1–Br4–Pb2	78.87(5)
Br6^1–Pb1–Br3	105.12(6)	Pb2–Br6–Pb1^2	80.14(5)
Br6–Pb2–Br5	89.79(6)	Pb2–Br3–Pb1	77.45(5)
Br6–Pb2–Br3	97.64(6)	Pb1–Br1–Pb2^1	79.03(5)
Br5–Pb2–Br3	87.35(7)	Pb2–Br5–Pb1	80.89(6)
^{1} −1 + x, +y, +z; ^{2} 1 + x, +y, +z			
Pro-Pb_3Br_{10}			
Br2–Pb2–Br1	82.34(5)	Br1–Pb1–Br2	81.74(5)
Br2–Pb2–Br3	83.38(4)	Br1^2–Pb1–Br2	95.35(5)
Br2–Pb2–Br4	87.93(6)	Br1^2–Pb1–Br2^2	81.74(5)
Br2–Pb2–Br4^1	163.99(5)	Br1–Pb1–Br1^2	175.39(9)
Br2–Pb2–Br5	93.28(6)	Br3–Pb1–Br2^2	172.72(6)
Br1–Pb2–Br3	78.53(5)	Br3^2–Pb1–Br2	172.72(6)
Br1–Pb2–Br4^1	84.30(5)	Br3^2–Pb1–Br2^2	83.35(4)
Br3–Pb2–Br4^1	85.36(6)	Br3–Pb1–Br2	83.35(4)
Br4–Pb2–Br1	97.06(5)	Br3^2–Pb1–Br1^2	81.41(5)
Br4–Pb2–Br3	170.70(5)	Br3–Pb1–Br1	81.41(5)
Br4–Pb2–Br4^1	102.462(15)	Br3–Pb1–Br1^2	101.88(6)
Br5–Pb2–Br1	174.47(4)	Br3^2–Pb1–Br1	101.88(6)
Br5–Pb2–Br3	97.68(6)	Br3^2–Pb1–Br3	90.91(7)
Br5–Pb2–Br4^1	99.48(5)	Pb2–Br2–Pb1	83.32(4)
Br5–Pb2–Br4	86.10(6)	Pb1–Br1–Pb2	81.02(4)
Br2^2–Pb1–Br2	102.71(7)	Pb1–Br3–Pb2	80.84(4)
Br1–Pb1–Br2^2	95.35(5)	Pb2–Br4–Pb2^3	164.41(8)
^{1} 1.5 − x, −0.5 + y, 1 − z; ^{2} 1 − x, y, 1 − z; ^{3} 1.5 − x, 0.5 + y, 1 − z			

Table S4. Parameters of C–H···Br contacts in the crystal structure of **Pro-Pb_3Br_{10}** and **Pro-$PbBr_3$**

D–H···A	D–H, Å	H···A, Å	D···A, Å	∠DHA, °	Symmetry codes
Pro-Pb_3Br_{10}					
*cat*1					
C2–H2···Br1	0.98	3.09	3.646(14)	117	-
C4–H4···Br1	0.97	3.10	3.994(15)	155	x, −1 + y, z
C2–H2···Br3	0.98	3.12	3.930(14)	142	1 – x, y, 1 – z
*cat*2					
C10–H10B···Br1	0.97	2.78	3.745(18)	174	1.5 – x, −0.5 + y, 1 – z
C9–H9A···Br5	0.97	2.94	3.88(2)	162	-
C7–H7···Br2	0.98	3.02	3.80(2)	137	x, −1 + y, z
C7–H7···Br5	0.98	3.02	3.662(14)	124	x, −1 + y, z
Pro-$PbBr_3$					
*cat*1					
C4–H4B···Br4	0.97	3.28	3.863(17)	120	2 – x, −0.5 + y, 1 – z
C1–H1···Br6	0.98	3.35	3.899(17)	117	x, y, 1 + z
C1–H1···Br5	0.98	2.86	3.78(2)	158	x, y, 1 + z
C3–H3A···Br5	0.97	3.19	3.98(2)	140	1 + x, y, 1 + z
C4–H4A···Br5	0.97	3.30	4.031(16)	133	1 + x, y, 1 + z
C2–H2D···Br2	0.97	2.95	3.887(19)	162	1 + x, y, 1 + z
*cat*2					
C9–H9B···Br2	0.97	3.28	3.917(16)	126	1 + x, y, 1 + z
C8–H8B···Br2	0.97	3.05	3.85(2)	141	1 + x, y, 1 + z
C8–H8B···Br4	0.97	3.22	3.79(2)	119	x, y, 1 + z
C9–H9A···Br3	0.97	3.26	3.765(18)	114	1 – x, 0.5 + y, 1 – z
C7–H7A···Br6	0.97	3.12	4.09(2)	176	1 – x, 0.5 + y, 1 – z
C9–H9A···Br6	0.97	3.12	3.870(16)	135	2 – x, 0.5 + y, 1 – z
C8–H8A···Br5	0.97	3.15	4.10(2)	168	1 – x, 0.5 + y, 1 – z
C7–H7B···Br5	0.97	3.04	3.91(2)	150	x, y, 1 + z

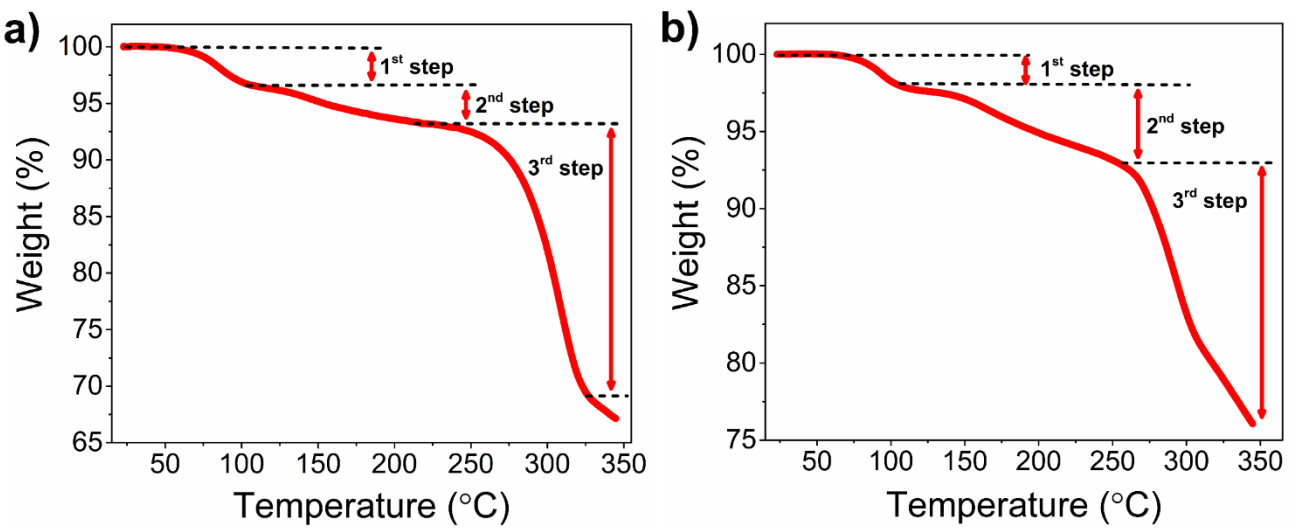

Figure S1. Thermogravimetric analysis of **Pro-Pb_3Br_{10} (a)** and (ProH)$PbI_3 \cdot H_2O$ **(b)** in nitrogen atmosphere.

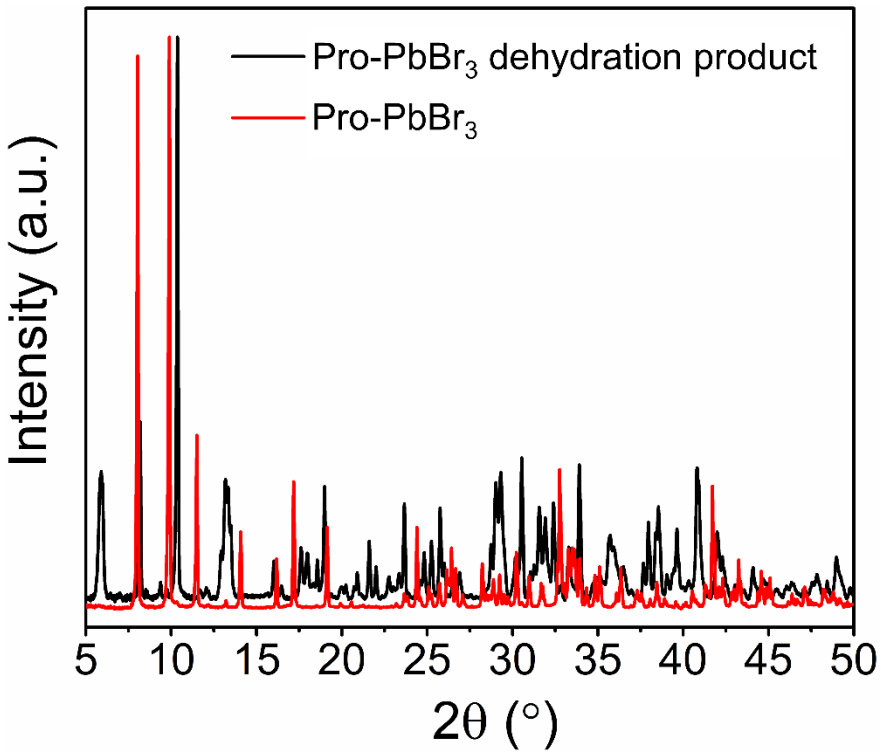

Figure S2. Powder X-ray diffraction pattern of **Pro-PbBr₃** before (red line) and after dehydration (black line)

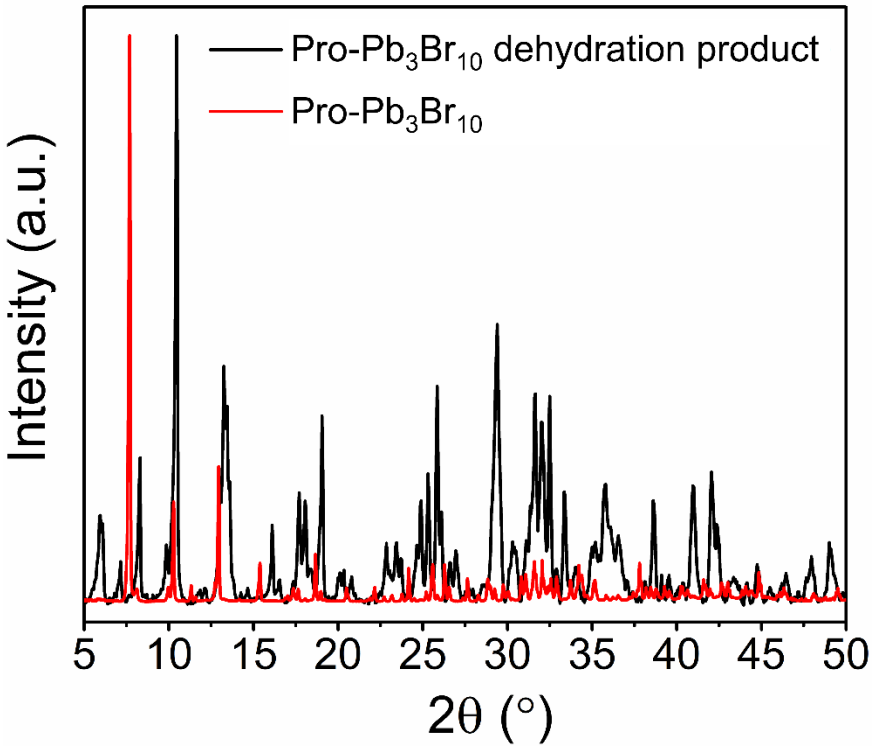

Figure S3. Powder X-ray diffraction pattern of **Pro-Pb₃Br₁₀** before (red line) and after dehydration (black line)

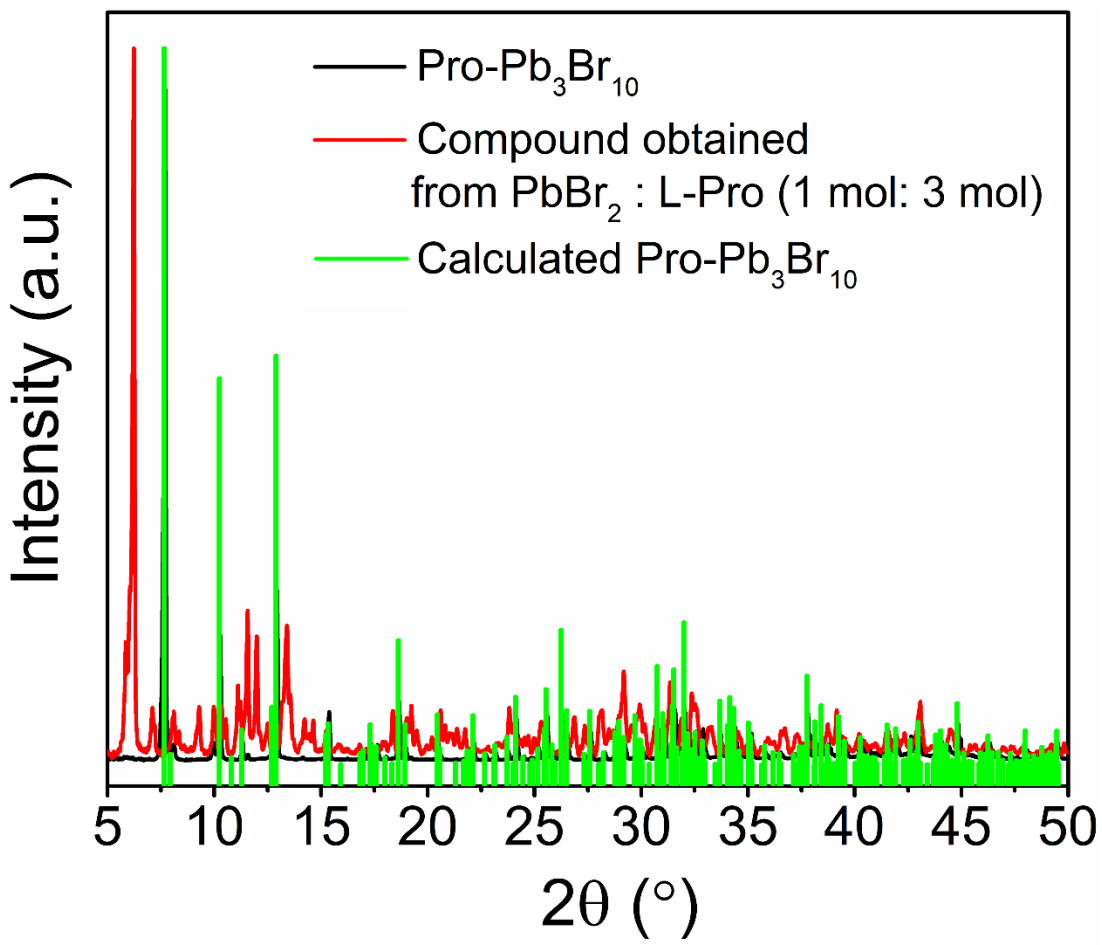

Figure S4. Powder X-ray diffraction pattern of **Pro-Pb_3Br_{10}** before dehydration (black line), product obtained with a 3-fold excess of L-Proline (red line) and **Pro-Pb_3Br_{10}** simulated from SXRD data.

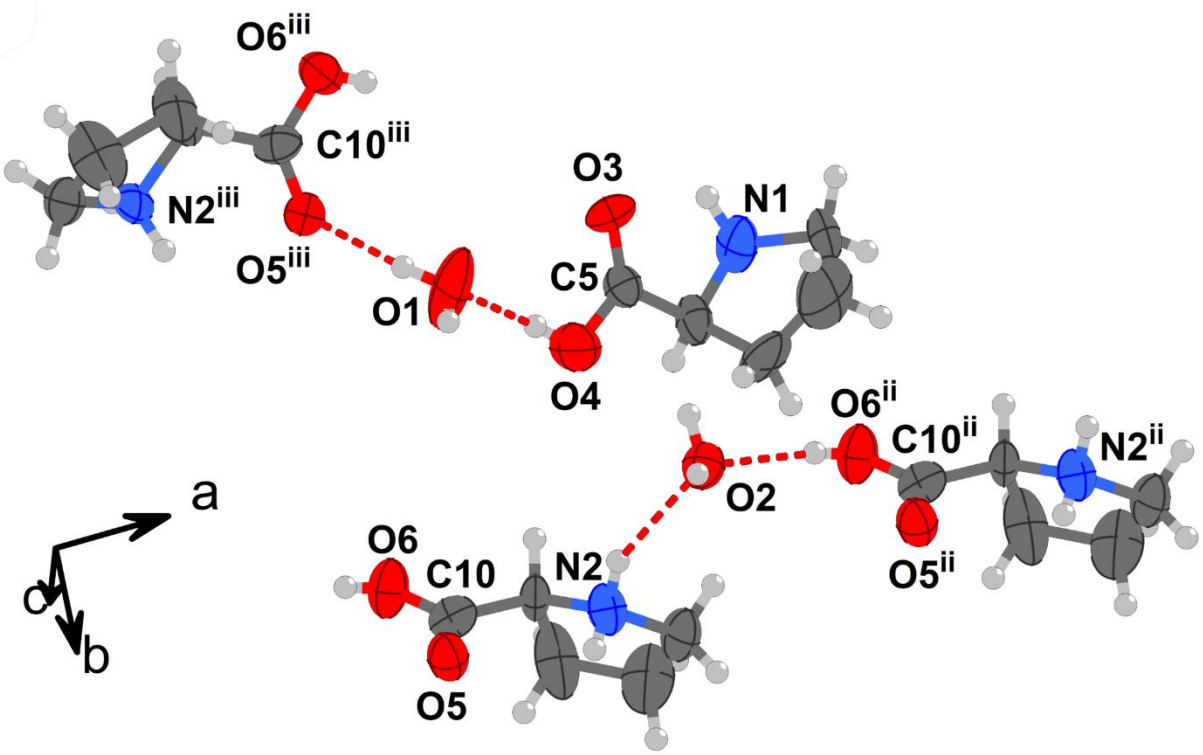

Figure. S5. Hydrogen bonding inside the organic layer of **Pro-$PbBr_3$**. Symmetry codes: (ii) 1 + x, y, z and (iii) −x, −0.5 + y, 1 – z.

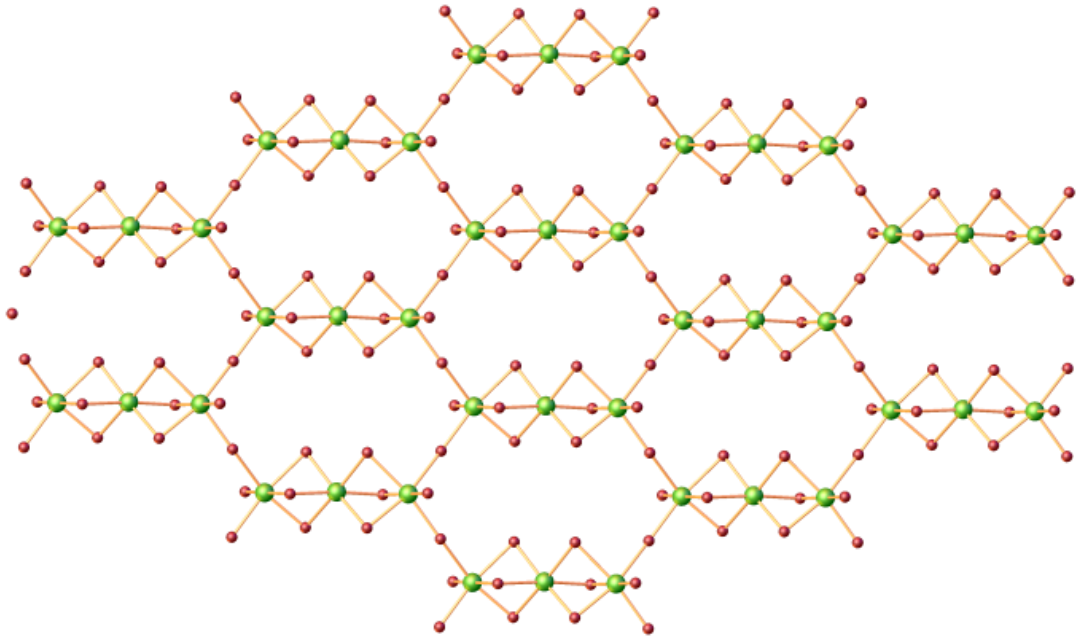

Figure. S6. 2D honeycomb-type inorganic sublattice of **Pro-Pb_3Br_{10}** viewed along *c*-axis.

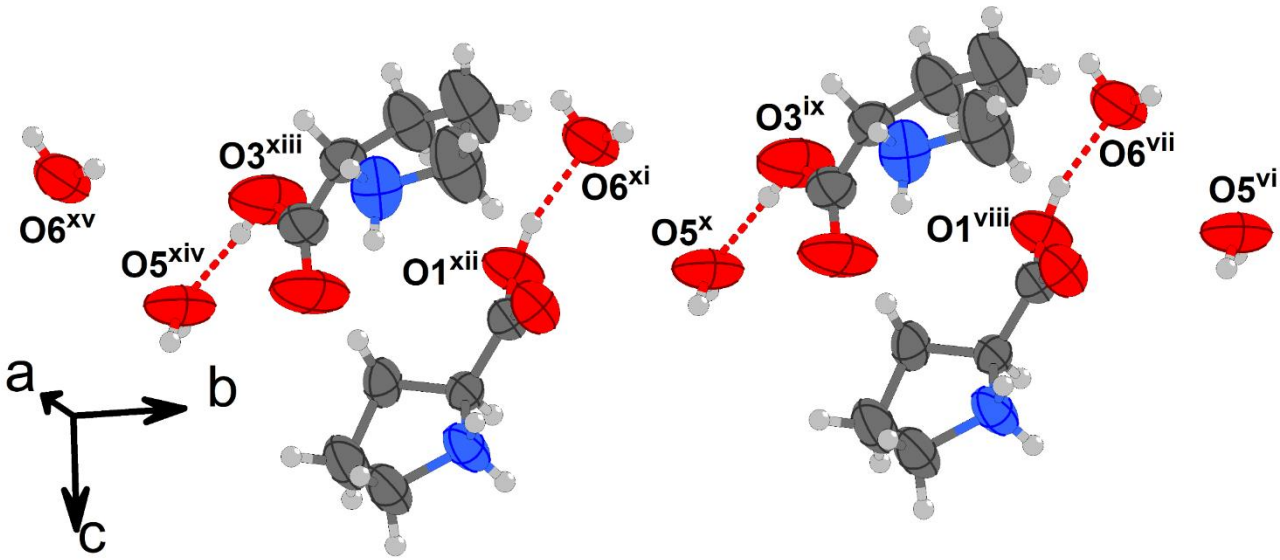

Figure. S7. Hydrogen bonds (red dashed lines) inside the organic part of **Pro-Pb_3Br_{10}**. The thermal ellipsoids are drawn at the 50% probability level. Symmetry codes: (vi) −0.5 + x, 0.5 + y, 1 + z; (vii) −0.5 + x, 0.5 + y, z; (viii) 0.5 − x, 0.5 + y, 2 − z; (ix) 0.5 − x, 0.5 + y, 1 − z; (x) −0.5 + x, −0.5 + y, 1 + z; (xi) −0.5 + x, −0.5 + y, z; (xii) 0.5 − x, −0.5 + y, 2 − z; (xiii) 0.5 − x, −0.5 + y, 1 − z; (xiv) −0.5 + x, −1.5 + y, 1 + z; (xv) −0.5 + x, −1.5 + y, z

Hirshfeld surface analysis

The Hirshfeld surface was derived using the data obtained from the single-crystal XRD analysis. All calculation were performed using a very high surface resolution with three-dimensional molecular surface created by mapping the normalized contact distance d_{norm} over colour range from red to blue (−0.484 to 1.164 for **Pro-$PbBr_3$** and −0.463 to 1.130 for **Pro-Pb_3Br_{10}**) (**Fig. S9**). The d_{norm} (**equation 1**) includes d_i (distance from the point to the nearest nucleus internal to the surface), d_e (distance from the point to the nearest nucleus external to the surface) and r^{vdW} (van der Waals radius of the appropriate atom internal or external to the surface) parameters.[63]

$$d_{norm} = \frac{d_i - r_i^{vdW}}{r_i^{vdW}} + \frac{d_e - r_e^{vdW}}{r_e^{vdW}} \qquad (1)$$

The value of d_{norm} is negative if contacts are shorter than vdW separations and positive for contacts greater than vdW separations.

Visualizations were performed using a red-white-blue colour scheme, where red highlights shorter contacts, white is used for contacts around vdW separation, and blue depicts longer contacts. The red spots on the 3D d_{norm} Hirshfeld surfaces indicate the direction and strength of the intermolecular E–H···Br hydrogen bonds (where E = N, O) or weak C–H···Br contacts. According to this, for compounds Pro-PbBr3 and **Pro-Pb_3Br_{10}** all the N–H···Br, O–H···Br hydrogen bonds are depicted as red spots on the 3D Hirshfeld surface (**Fig. S8**). At the same

time, only C1–H1···Br5 and C2–H2D···Br2 contacts for **Pro-$PbBr_3$**, C10–H10···Br1 and C9–H9···Br5 contacts for **Pro-Pb_3Br_{10}** are shown as red spots indicating the distances shorter than van der Waals radii of corresponding atoms, while the remaining C–H···Hal contacts for these perovskites are depicted as white spots on the 3D Hirshfeld surface (**Fig. S8**). The C···Br contacts are also observed in 3D d_{norm} Hirshfeld surfaces with d(C···Br) = 3.4415(220) Å which is shorter than sum of van der Waals radii of corresponding elements (r_{vdW}(Br) = 1.85 Å and r_{vdW}(C) = 1.7 Å, r_{vdW}(Br) + r_{vdW}(C) = 3.55 Å). The C···Br contacts are depicted as red dashed line in **Fig. S8**.

The two-dimensional fingerprint plots show the occurrence of different kinds of intermolecular contacts in the form of griddle-coloured areas in each of d_i and d_e in the range from 0.4 to 3.0 Å (**Fig. S9, S10**). Also, the percentage contributions of all the individual interactions of compounds **Pro-$PbBr_3$** and **Pro-Pb_3Br_{10}** are calculated and shown as a 3D pie chart in **Fig. S11**.

The major part in the fingerprint plots is covered by Br···H interactions which are 87.30% and 91.50% for **Pro-$PbBr_3$** and **Pro-Pb_3Br_{10}**, respectively. The Br···O and Br···C interactions cover the area of 4.00 and 1.60%, respectively for compound **Pro-$PbBr_3$** while for compound **Pro-Pb_3Br_{10}** these interactions cover the slightly lower area of 2.70 and 0.90%, respectively.

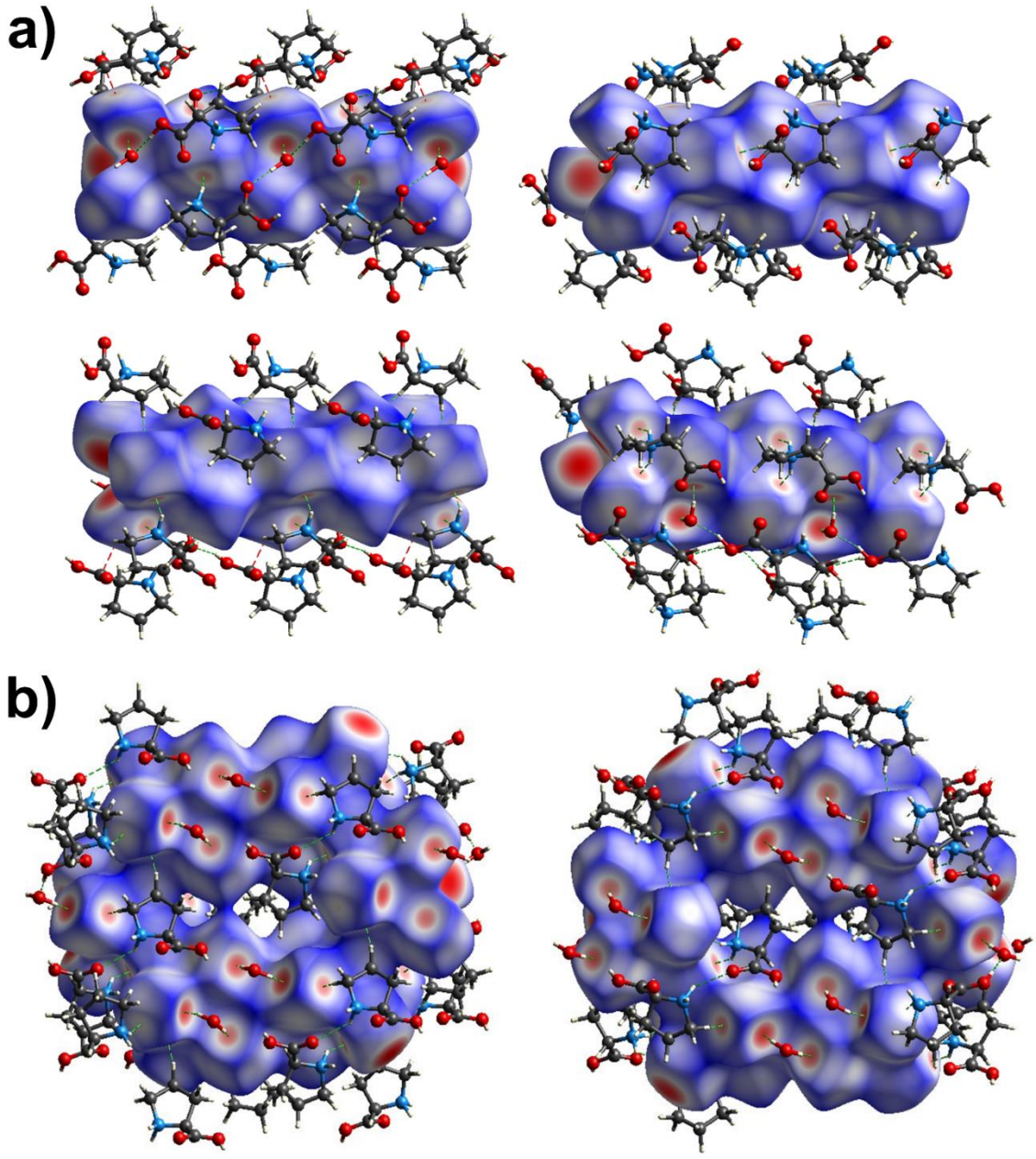

Figure. S8. View of the d_{norm} quantity mapped on the Hirshfeld surface of **(a)** $[Pb_4Br_{12}]^{4-}$ inorganic fragment of hybrid perovskite **Pro-PbBr$_3$** and **(b)** $[Pb_8Br_{19}]^{3-}$ inorganic fragment of hybrid perovskite **Pro-Pb$_3$Br$_{10}$**. The red color represents the area on the surface where the atoms make intermolecular contacts closer than the sum of their van der Waals radii. The O–H···Br, N–H···Br hydrogen bonds and C–H···Br weak contacts are indicated as a green dashed line.

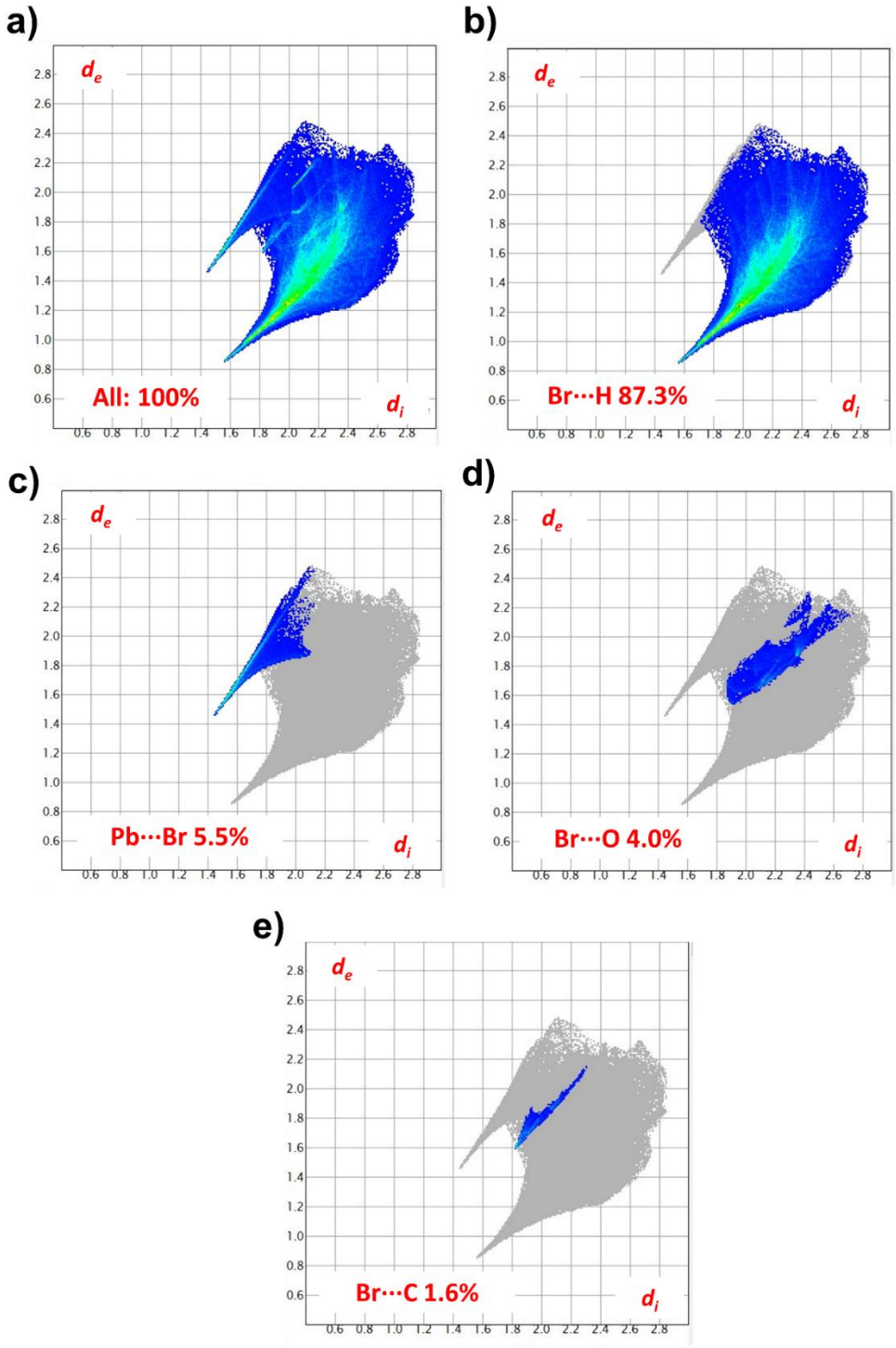

Figure S9. 2D fingerprint plots of the intermolecular contacts in the compound **Pro-PbBr$_3$**. The full fingerprint appears beneath each decomposed plot as a grey shadow.

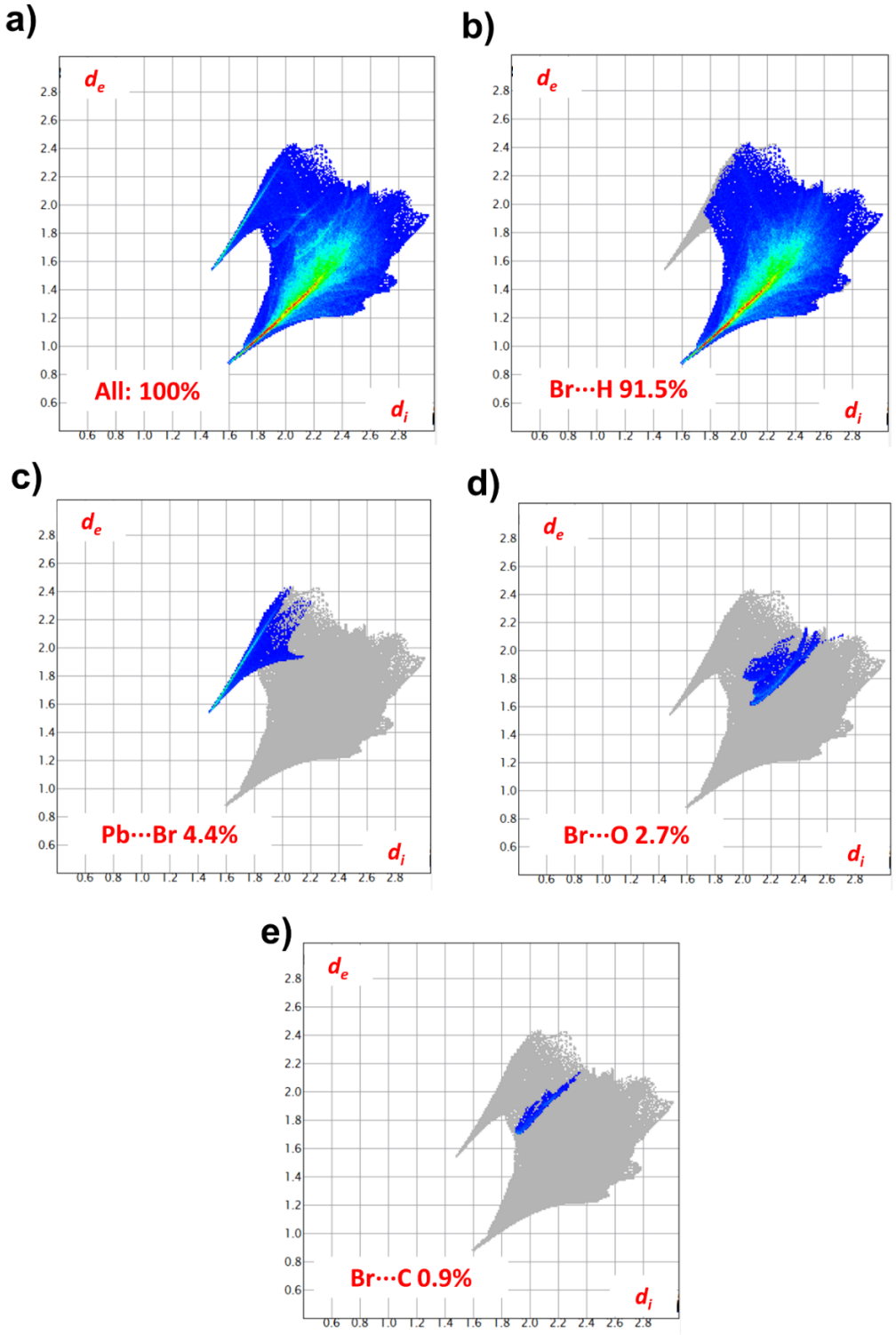

Figure S10. 2D fingerprint plots of the intermolecular contacts in the compound **Pro-Pb_3Br_{10}**. The full fingerprint appears beneath each decomposed plot as a grey shadow.

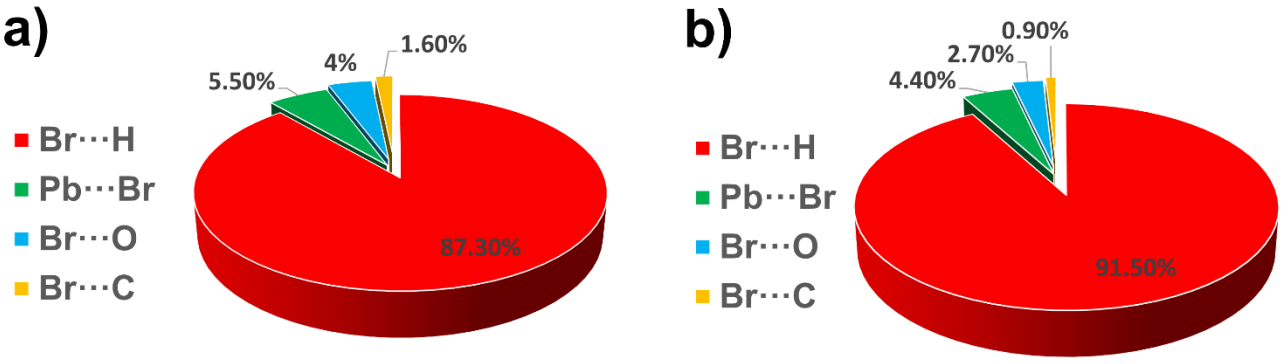

Figure S11. Pie chart showing relative contribution to the Hirshfeld surface for the major intermolecular contacts in compounds **Pro-$PbBr_3$ (a)** and **Pro-Pb_3Br_{10} (b)**

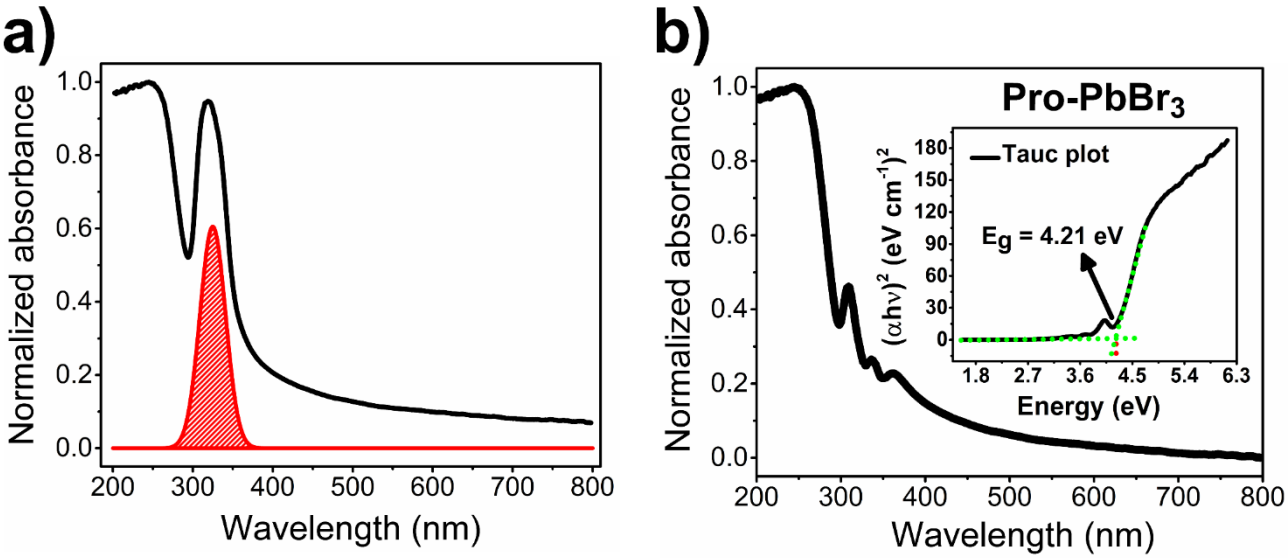

Figure S12. The normalized solid-state optical absorbance spectrum of **Pro-$PbBr_3$** (black line) along with the peak modeled using a Gaussian function (red line), which was subsequently subtracted from the absorption spectrum **(a)**; The normalized solid-state optical absorbance spectrum of **Pro-$PbBr_3$** (black line) obtained after subtracting the modeled peak which was used to determine the band gap value of this hybrid perovskites. The corresponding Tauc plot is shown as an inset.

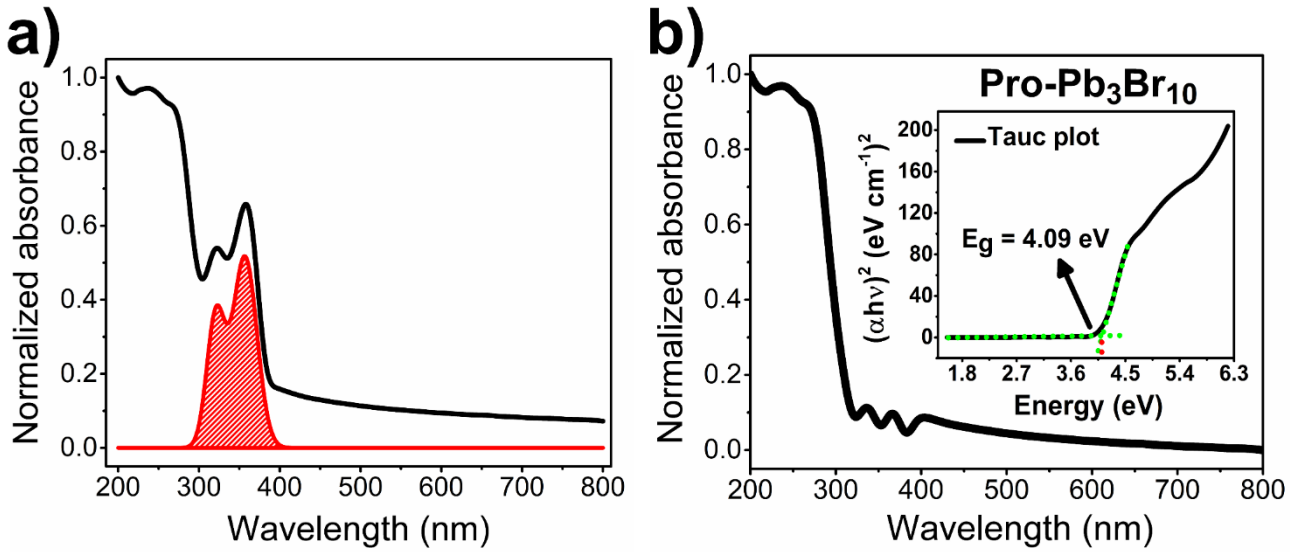

Figure S13. The normalized solid-state optical absorbance spectrum of **Pro-Pb_3Br_{10}** (black line) along with the peaks modeled using a Gaussian function (red line), which were subsequently subtracted from the absorption spectrum **(a)**; The normalized solid-state optical absorbance spectrum of **Pro-Pb_3Br_{10}** (black line) obtained after subtracting the modeled peaks which was used to determine the band gap value of this hybrid perovskites. The corresponding Tauc plot is shown as an inset.

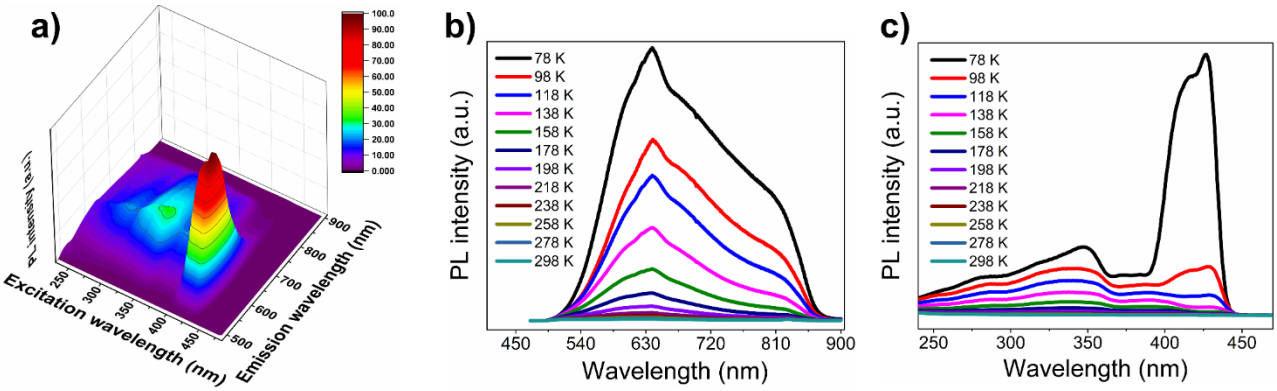

Figure S14. 3D photoluminescence spectra at 78 K of a powder sample of (ProH)$PbI_3 \cdot H_2O$ **(a)**; Temperature-dependent 2D emission spectra of (ProH)$PbI_3 \cdot H_2O$ **(b)**; Temperature-dependent 2D excitation spectra of (ProH)$PbI_3 \cdot H_2O$ **(c)** hybrid perovskite;

References:

1 Y. Y. Li, C. K. Lin, G. L. Zheng, Z. Y. Cheng, H. You, W. D. Wang and J. Lin, *Chem. Mater.*, 2006, **18**, 3463–3469.

2 Y. Zheng, J. Xu and X. H. Bu, *Adv. Opt. Mater.*, 2022, **10**, 1–7.

3 A. Kaltzoglou, C. C. Stoumpos, A. G. Kontos, G. K. Manolis, K. Papadopoulos, K. G. Papadokostaki, V. Psycharis, C. C. Tang, Y. K. Jung, A. Walsh, M. G. Kanatzidis and P. Falaras, *Inorg. Chem.*, 2017, **56**, 6302–6309.

4 Z. Li, M. A. Najeeb, L. Alves, A. Z. Sherman, V. Shekar, P. Cruz Parrilla, I. M. Pendleton, W. Wang, P. W. Nega, M. Zeller, J. Schrier, A. J. Norquist and E. M. Chan, *Chem. Mater.*, 2020, **32**, 5650–5663.

5 M. D. Smith, B. L. Watson, R. H. Dauskardt and H. I. Karunadasa, *Chem. Mater.*, 2017, **29**, 7083–7087.